Short title: Visualizing protein-protein interactions in planta via delocalization

The author for contact details is Daniël Van Damme (daniel.vandamme@psb.vib-ugent.be).

Rapamycin-dependent delocalization as a novel tool to reveal protein-protein interactions in plants

Joanna Winkler[1,2], Evelien Mylle[1,2], Andreas De Meyer[1,2], Benjamin Pavie[3], Julie Merchie[1,2], Peter Grones[1,2], Daniel Van Damme[1,2,#]

[1] Ghent University, Department of Plant Biotechnology and Bioinformatics, Technologiepark 71, 9052 Ghent, Belgium
[2] VIB Center for Plant Systems Biology, Technologiepark 71, 9052 Ghent, Belgium
[3] VIB BioImaging Core, Ghent, Belgium.
corresponding author

One-sentence summary: rapamycin-dependent delocalization allows quantifying protein-protein interactions inside plant cells.

Author contributions: DVD initiated the project and designed experiments. JW, EM, ADM and PG designed and performed experiments. BP wrote the script for quantification of the data. JM performed experiments. JW, PG and DVD wrote the paper.

Abstract

Identifying protein-protein interactions (PPI) is crucial to understand any type of biological process. Many PPI tools are available, yet only some function within the context of a plant cell. Narrowing down even further, only few PPI tools allow visualizing higher order interactions. Here, we present a novel and conditional *in vivo* PPI tool for plant research. Knocksideways in plants (KSP) uses the ability of rapamycin to alter the localization of a bait protein and its interactors via the heterodimerization of FKBP and FRB domains. KSP is inherently free from many limitations, which other PPI systems hold. It is an *in vivo* tool, it is flexible concerning the orientation of protein tagging as long as this does not interfere with the interaction and it is compatible with a broad range of fluorophores. KSP is also a conditional tool and therefore does not require additional controls. The interactions can be quantified and in high throughput

by the scripts that we provide. Finally, we demonstrate that KSP can visualize higher-order interactions. It is therefore a versatile tool, complementing the PPI methods field with unique characteristics and applications.

Keywords: protein-protein interaction, knocksideways, KSP, rapamycin, FKBP-FRB

Introduction

Unravelling macromolecular complexes and interaction networks among proteins plays a pivotal role in understanding biological processes. In the past 20 years, the number of articles which feature protein-protein interactions (PPIs) as a topic or focusing on PPI technology development has been steadily increasing (Xing et al., 2016). Although a plethora of tools to investigate PPIs is available (Miura, 2018; Titeca et al., 2019; Wiens and Campbell, 2018), those which can be used *in planta* are relatively limited (Fukao, 2012; Lampugnani et al., 2018; Struk et al., 2019; Xing et al., 2016). In plant systems, including *Arabidopsis thaliana*, multiple interactomes have been described based on large-scale screenings (Arabidopsis Interactome Mapping Consortium, 2011; Boruc et al., 2010a; Jones et al., 2014; Piya et al., 2014). Interactomes plot the landscape surrounding a certain bait protein, yet seldom provide information on specific or direct interaction partners. The evaluation of specific biological functions and the mode of action of a protein of interest usually requires multi-technical approaches (Struk et al., 2019). Thus, a proper selection of the optimal PPI tools to use represents a foremost important task.

Affinity-purification (AP), including co-immunoprecipitation (Co-IP) and tandem affinity purification (TAP), followed by mass spectrometry (MS) experiments (Masters, 2004; Ransone, 1995; Rigaut et al., 1999) can be positioned in between *in vivo* and *in vitro* experimental approaches. These are commonly used powerful screening tools to identify novel PPIs. One advantage is that the interactions occur in their physiological environment (Rubio et al., 2005; Xing et al., 2016). However, AP/MS requires a cell lysis step, during which it is possible to impose false-positive PPIs, and even more common, to disrupt weak ones (Miteva et al., 2013). On the contrary, with proximity – labelling methods, there is no need to preserve PPIs during lysis and extraction. Proximity – dependent biotin identification (BioID) allows to preserve spatial conditions of PPIs and is particularly useful for low-affinity and transient interactions (Roux et

al., 2012) also in plants (Arora et al., 2019; Branon et al., 2018; Conlan et al., 2018; Das et al., 2019; Khan et al., 2018; Lin et al., 2017; Mair et al., 2019; Zhang et al., 2019).

The assays using the yeast *Saccharomyces cerevisiae*, like Yeast two-hybrid (Y2H) system (Fields and Song, 1989; Wen, 2014), rely on the reconstitution of bipartite transcriptional activators (Lampugnani et al., 2018). Y2H can be upgraded into Yeast three-hybrid (Y3H), which brings the system to the tripartite-protein interaction level (Alberti et al., 2007; Cottier et al., 2011; Maruta et al., 2016). Also, incorporating Y2H with next-generation sequencing (NGS) or recombination based Y2H 'library vs library' screening (Erffelinck et al., 2018; Yang et al., 2018) resulted in elaborate, high-throughput PPIs screens tools. Nevertheless, as yeasts lack certain chaperones or posttranslational modifications occurring *in planta*, identifying interactions, which rely on those, is not feasible. In addition, proteins might require several other ones to stabilize their interaction. For instance, the octameric endocytic TPLATE complex has been shown as a very robust multi-subunit complex via proteomics analysis, but there was only one interaction which could be identified in yeast (Gadeyne et al., 2014). Finally, yeasts assays do not provide any information about the subcellular localization of the PPI.

Bimolecular Fluorescence Complementation (BiFC) is a versatile tool which relies on the ability of complementary halves of fluorescent proteins (FP) to reconstitute their properties upon PPI (Ghosh et al., 2000). BiFC was adapted for plant systems (Bracha-Drori et al., 2004; Hu et al., 2002; Walter et al., 2004), optimized for ratiometric imaging (Grefen and Blatt, 2012) and also developed into tripartite split-GFP in order to avoid self-assembly (Cabantous et al., 2013) or to visualize triple interactions (Offenborn et al., 2015). Weak and transient PPIs can be visualized using via these methods as once FP halves re-assemble, the interaction is locked. Interaction is irreversible and interacting proteins are thus artificially stabilized, and remain in close proximity (Magliery et al., 2005), regardless of localization and time of interaction, which is one of the biggest limitations of this system. Therefore, both techniques require multiple negative controls, as well as testing multiple combinations of orientations of the split-GFP proteins tags.

Förster resonance energy transfer (FRET) is one of the *in vivo* assays *in planta* where interplay between two proteins of interested can be measured among others by using fluorescence lifetime imaging (FLIM) (Förster, 1948; Gadella et al., 1993; Sun et al., 2011; Xing et al., 2016). Recently FRET-FLIM has been developed into a three-fluorophore system which enabled to

visualize triple PPIs (Glöckner et al., 2019). Nevertheless, FRET-FLIM is quite-labor intense, requires careful interpretation and multiple control assays. Moreover, is it significantly limited by the intrinsic properties of the FPs (Bhat et al., 2006; Struk et al., 2019).

Here, we present a PPI tool we named Knocksideways in plants (KSP), which can be compared to an intracellular Co-IP experiment. The tool relies on the rapamycin-induced heterodimerization between the FKBP domain of FKBP12 (FKBP) and the FKBP12 rapamycin binding domain of mTOR (FRB). This dimerization tool is well-established and successfully used in human, animal, plasmodium and yeast (Haruki et al., 2008; Putyrski and Schultz, 2012; Wood et al., 2017; Chojnowski et al., 2018; Hughes and Waters, 2017; Nomura et al., 2018; Putyrski and Schultz, 2012) and has occasionally also been used in plants (Li et al., 2011; Rosenfeldt et al., 2008). We were inspired by the Knocksideways (KS) approach in animal cells, which combines conditional FKBP-FRB binding with rerouting proteins to the mitochondria (Robinson et al., 2010). This type of 'drag-away' technique has already been explored PPIs in plant research. For instance, the Nuclear Translocation Assay (NTA), the Cytoskeleton-based localization Assay for Protein-Protein Interaction (CAPPI) and the Modification of Intracellular Localization (MILo) work via a similar approach (Dixon and Lim, 2010; Kaplan-Levy et al., 2014; Lv et al., 2017). Nevertheless, both tools are not conditional and their subcellular targeting options reported so far, are limited. In this study, we focused on introducing KS *in planta*, expanding the availability of the subcellular FRB anchors and developing the system into a higher-order PPI tool where the results can be quantified.

Results

Rapamycin efficiently relocalizes FKBP-fusions to FRB-tagged subcellular compartments in planta

First, we tested if rapamycin-induced FKBP-FRB domains heterodimerization is efficient in plants. To do this, we amplified the FRB* domain from MAPPER (Chang et al., 2013) and fused it with various peptides, anchoring it at different subcellular locations. This enriches the tool's application for diversely localized proteins of interest. ARABIDOPSIS THALIANA MICROTUBULE END BINDING PROTEIN EB1A (*At*EB1a), a plus-end microtubule marker (Van Damme et al., 2004) was used to design the microtubular anchor EB1a-TagBF2-FRB*. We fused

the FRB* domain to a nuclear localization signal, NLS-TagBFP2-FRB* to create a nuclear-localized anchor. The N-terminal part of the Ca^{2+}-dependent protein kinase CPK34, containing a myristoylation/palmitoylation signal responsible for plasma membrane (PM) protein localization (Kirik et al., 2012; Myers et al., 2009), was used to create MYRI-TagBFP2-FRB* and target FRB to the PM. Finally, for mitochondrial targeting, we used yeast mitochondrial outer membrane protein Tom70p (MITO-TagBFP2-FRB*), previously reported to be functional in mammalian cells (Kessels and Qualmann, 2002; Robinson et al., 2010). All constructs used are available as gateway building blocks (Supplemental Figure 1).

We expressed the aforementioned FRB* constructs into *Nicotiana benthamiana* abaxial leaf cells and used spinning disk confocal microscopy to visualize the fusion proteins. All FRB* constructs localized at their expected subcellular localization. We then combined these with assorted mCherry-FKBP-tagged proteins, and monitored their localization prior and after rapamycin treatment. TPLATE is a subunit of the octameric TPLATE complex (TPC) involved in clathrin-mediated endocytosis (Gadeyne et al., 2014). In *N. benthamiana,* over expressed TPLATE primary localizes ubiquitously in the cytoplasm (Gadeyne et al., 2014), similar to our TPLATE-mCherry-FKBP (Figure 1A). After rapamycin treatment, TPLATE was re-routed to the microtubules (MTs) in the presence of EB1a-TagBFP2-FRB* (Figure 1A). MICROTUBULE-ASSOCIATED PROTEIN 65-1 (MAP65-1) is a MTs cross-linker (Tulin et al., 2012; Van Damme et al., 2004). In the presence of the microtubule depolymerizing agent oryzalin, rapamycin can delocalize and trap MAP65-1 in the nucleus via binding to NLS-TagBFP2-FRB* (Figure 1B). Similar to what has been reported before (Boruc et al., 2010a; Spinner et al., 2013), mCherry-FKBP fusions of the protein phosphatase 2A regulatory subunit RCN1 and the cyclin-dependent kinase CELL DIVISION CONTROL 2 (CDKA;1) were largely cytoplasmic in the absence of the dimerizer. Rapamycin delocalized RCN1 to the plasma membrane-docked MYRI-TagBFP2-FRB* (Figure 1C) and pulled CDKA;1 to the mitochondria in the presence of MITO-TagBFP2-FRB* (Figure 1D).

We observed, that MITO-TagBFP2-FRB*-labeled structures differed in size, and occasionally clustered into larger structures. To confirm that the punctate MITO-TagBFP2-FRB* signals indeed represent mitochondria, we expressed MITO-TagBFP2-FRB* in *N. benthamiana* leaves and stained them with the mitochondrial dye MitoTracker™ Red. The staining colocalized with the MITO-TagBFP2-FRB* regardless of clustering (Supplemental Figure 2A). Additionally, to

exclude that clustering might affect FKBP-fused protein localization, we co-infiltrated MITO-TagBFP2-FRB* with the mCherry-FKBP-tagged transcription factor LONESOME HIGHWAY (LHW-mCherry-FKBP). In the presence of rapamycin, LHW-mCherry-FKBP was re-routed to the mitochondria irrespective of their aggregation status (Supplemental Figure 2B).

Taken together, our results showed that heterodimerization of FKBP-FRB* upon rapamycin addition works efficiently in plants, and that the system is capable of localizing baits to different subcellular FRB*-anchors.

Knocksideways is a robust, quantitative protein-protein interaction tool *in planta*

We then used KSP to visualize PPIs in *N. benthamiana*. To do so, we targeted our FRB* domain to a specific subcellular location. We fused several bait proteins, with different subcellular localizations and from different functional classes, to mCherry-FKBP. We expressed these together with their GFP-fused interaction partners and monitored their localization in the absence and presence of rapamycin. We designed Fiji/ImageJ-compatible scripts allowing to easily quantify nuclear and mitochondrial delocalization upon rapamycin addition (see materials and methods and Supplemental document 1 for a detailed description on how to use the scripts).

To demonstrate that rapamycin itself does not cause arbitrary binding or random delocalization of proteins, we co-infiltrated eGFP together with TPLATE-mCherry-FKBP and MITO-TagBFP2-FRB*. Without rapamycin, both eGFP and TPLATE-mCherry-FKBP localized ubiquitously in the cytosol. Rapamycin addition effectively delocalized TPLATE to the mitochondria and mitochondrial clusters but did not affect the localization of eGFP (Figure 2A). We quantified the mitochondria/cytoplasm intensity ratio in untreated and rapamycin-exposed samples using our MitTally script (Mitochondria Tally marks; see Supplemental document 1). Statistical analysis performed with ANOVA to account for heteroscedasticity indicates that contrary to eGFP, TPLATE intensity at the mitochondria was significantly increased after rapamycin treatment (Figure 2A i).

SAC51-LIKE (SACL) is a bHLH transcription factor, which heterodimerizes with LONESOME HIGHWAY (LHW) (Vera-Sirera et al., 2015). The SACL/LHW interaction has been demonstrated

via various conventional PPI methods including immunoprecipitation followed by tandem mass spectrometry (IP-MS/MS), yeast two-hybrid (Y2H) and Förster resonance energy transfer (FRET-FLIM) (De Rybel et al., 2013; Ohashi-Ito and Bergmann, 2007; Vera-Sirera et al., 2015). Here, we tested SACL-GFP and LHW-mCherry-FKBP in KSP with MITO-TagBFP2-FRB*. Without rapamycin, SACL and LHW are nuclear. Rapamycin treatment delocalized both proteins to the mitochondria, thereby confirming their interaction in our system and independent of the nuclear environment. (Figure 2B).

Phosphorylation of the transcription factor BRI1-EMS-SUPPRESSOR 1 (BES1) by the BRASSINOSTEROID-INSENSITIVE 2 (BIN2) kinase is a well-established interaction in the brassinosteroid signaling pathway (Anwar et al., 2018; Planas-Riverola et al., 2019). We co-infiltrated BES1-GFP with BIN2-mCherry-FKBP and MITO-TagBFP2-FRB*. Without rapamycin, BIN2 is primarily nuclear while BES1 is ubiquitously present in the cytoplasm. Rapamycin locks BIN2 at the mitochondria where it recruits BES1 (Figure 2C).

The TPLATE complex core consists of four subunits named TPLATE, TML, LOLITA and TASH3 and interactions between particular subunits have been demonstrated via different PPI methods (Gadeyne et al., 2014; Hirst et al., 2014). We tested the TPLATE-TML interaction, previously reported to interact via split-GFP and co-IP (Gadeyne et al., 2014) using KSP. Both TPLATE-mCherry-FKBP and TML-GFP are largely cytoplasmic when over expressed in *N. benthamiana*. Exposure to rapamycin reroutes TPLATE together with TML to the mitochondria, reaffirming their interaction. Interaction is robust, and affects the mitochondria/cell intensity ratio significantly (Figure 2D).

To test if visualization of PPI via KSP is compatible with other subcellular locations, we investigated the efficiency of NLS-TagBFP2-FRB* as anchor. Rapamycin rerouted TPLATE-mCherry-FKBP into the nucleus, together with TML-GFP (Figure 3A a-h). We quantified the nucleus/cytoplasm intensity ratio in untreated and rapamycin-exposed samples using our NucTally script (Nuclear Tally marks; see Supplemental document 1). The nucleus/cytoplasm median intensity ratio, indicative for the accumulation of TPLATE/TML in the nucleus, increased significantly upon treatment (Figure 3A i). Next, we co-infiltrated MAP65-1-GFP with MAP65-1-mCherry-FKBP and NLS-TagBFP2-FRB*. Prior to rapamycin treatment, both MAP65-1 constructs localize predominantly on microtubules, although the GFP-fusion, likely due to over expression, possessed an increased propensity for aggregation compared to the mCherry-FKBP fusion.

After the treatment with rapamycin and oryzalin, MAP65-1 constructs were released from the microtubules and both constructs significantly co-delocalized to the nucleus (Figure 3B and Figure 3B i), while oryzalin treatment alone did not forced proteins into the nucleus (Supplemental Figure 3).

The above examples demonstrate that KSP is inducible and feasible at various subcellular locations. It allows visualizing PPI of different biological nature using different subcellular anchor points. Finally, PPI can be quantified with our MitTally and NucTally scripts, which generate delocalization ratios that allow statistical analysis of the interaction.

KSP works fast and remains stable for several hours

To investigate the required timing for KSP to occur in *N. benthamiana*, leaves co-expressing BES1-GFP, BIN2-mCherry-FKBP and MITO-TagBFP2-FRB* were treated with rapamycin and the delocalization was monitored at different time points. Interaction through delocalization was visible as soon as five minutes after rapamycin treatment (Supplemental Figure 4A). This time is the minimal time required for preparing the sample, mounting it on the microscope and finding the proper focal plane. Further, we co-infiltrated another interaction pair, SACL3-GFP, LHW-mCherry-FKBP and MITO-TagBFP2-FRB*, added rapamycin and checked proteins localization after one hour and after 24hrs in the greenhouse. SACL3/LHW rerouting to the mitochondria was clearly visible within one hour following treatment and remained stable over time (Supplemental Figure 4B). These two examples indicate that KSP allows PPI visualization over a broad time window. Interactions occur rapidly, and at the same time they are long lasting, hence visualization can be flexible.

Knocksideways does not stabilize protein-protein interactions

KSP allowed to reproduce interactions reported before (Anwar et al., 2018; De Rybel et al., 2013; Gadeyne et al., 2014; Ohashi-Ito and Bergmann, 2007; Planas-Riverola et al., 2019; Tulin et al., 2012; Vera-Sirera et al., 2015). However, we also encountered protein pairs, which did not interact in our system. One canonical interaction, which we tested and that does not work

in our system is KIP-RELATED PROTEIN 2 (KRP2)/CELL DIVISION CONTROL 2 (CDKA;1) (Boruc et al., 2010a). We co-infiltrated KRP2-GFP with CDKA;1-mCherry-FKBP and MITO-TagBFP2-FRB*. CDKA;1 was effectively rerouted to mitochondria after rapamycin treatment (Figure 1D andSupplemental Figure 5A), yet KRP2-GFP remained nuclear (Supplemental Figure 5A). The PP2A subunit RCN1-mCherry-FKBP can delocalize to both the plasma membrane via MYRI-TagBFP2-FRB* (Figure 1C) and to the mitochondria with MITO-TagBFP2-FRB* (Supplemental Figure 5B). The interaction between the PP2A regulatory A subunit RCN1 and the PP2A regulatory B subunit FASS was previously shown via BiFC and tandem affinity purification (TAP) (Spinner et al., 2013). Here, we were not able to replicate this interaction as GFP-FASS was not rerouted to the FRB* anchor together with RCN1 (Supplemental Figure 5B). Recently, the interplay between CLATHRIN LIGHT CHAIN 1 (CLC1) and AUXILIN-LIKE1 (AUXL1) has been established *in planta* via BiFC (Adamowski et al., 2018). We co-infiltrated GFP-AUXL1 with CLC1-mCherry-FKBP and MITO-TagBFP2-FRB*. Rapamycin relocalizes CLC1 to the mitochondria without affecting the localization of AUXL1 (Supplemental Figure 5C). At this point, it remains unclear why we could not confirm these previously reported interactions. Sterical hindrance of our mCherry-FKBP tag, the requirement of a specific subcellular localization, or additional partners for interactions to occur are likely possibilities. As our system does not stabilize PPI, KSP might also be discriminating the visualization of strong from weak or timely interactions.

Knocksideways allows to visualize higher order infiltrations *in planta*

TPLATE, TML, LOLITA and TASH3, are part of the TPC core and using either one of these as bait retrieves the others as prey in APMS experiments (Gadeyne et al., 2014; Hirst et al., 2014). Whereas interaction between TPLATE and TML could be established using KSP (Figure 2D and Figure 3A), the smallest TPC core subunit, LOLITA-GFP, was however not rerouted to the mitochondria when combined with TPLATE-mCherry-FKBP and MITO-TagBFP2-FRB* (Figure 4A). LOLITA and TASH3 have been previously reported as the only TPC pair interacting in yeast (Gadeyne et al., 2014). We therefore decided to repeat the LOLITA/TPLATE interaction assay in KPS in the presence of TASH3. To avoid possible fluorophore cross talk during spinning disk confocal microscopy, we cloned a fluorophore-less mitochondrial anchor MITO-FRB*. Consequently, we used KPS in a ternary combination and co-infiltrated LOLITA-GFP, TPLATE-

mCherry-FKBP, TASH3-TagBFP2 and MITO-FRB*. Without rapamycin, the localization pattern of the fluorescently labeled constructs was omnipresent, with LOLITA also displaying a strong nuclear localization. In contrast to our previous experiment, addition of rapamycin now rerouted all three TPC subunits to the mitochondria (Figure 4B). This indicates that all three proteins interact and that the TPLATE/LOLITA interaction requires stabilization via TASH3. We conclude that KSP allows to visualize higher-order, linear interactions and provides a possibility to increase our structural insight into multi-protein complexes.

Discussion

Rapamycin-induced FKBP-FRB heterodimerisation is feasible *in planta*

Rapamycin-dependent rerouting of FKBP-tagged proteins to FRB-tagged mitochondria (KS, Knocksideways) results in their rapid inactivation. This kind of approach was first used to demonstrate role of AP-1 in retrograde trafficking (Robinson et al., 2010). To our knowledge, the FKBP-FRB-rapamycin system has so far not been widely employed in plants. It has been used to investigate Arabidopsis cryptochrome 2 activity upon chemical induction (Rosenfeldt et al., 2008). Additionally, Arabidopsis FRB (AtFRB) and human FKBP (HsFKBP) were used to test the feasibility of the split-luciferase assay (SFLC) to monitor the dynamics of PPI in plant cells (Li et al., 2011). Compared to other fields, *in planta* tools available to investigate protein-protein interactions are relatively limited. Here, we describe KS for plants (KSP) in the *N. benthamiana* transient expression assay,), which we developed into a novel, inducible PPI tool holding a unique set of features.

We show that rerouting various proteins to distinct subcellular localizations is feasible in our system. Other 'anchor-away' techniques like NTA, CAPPI and MILo (Dixon and Lim, 2010; Kaplan-Levy et al., 2014; Lv et al., 2017), are limited in terms of subcellular rerouting options due to their direct fusion with the anchor. In contrast, KSP easily combines with multiple anchors without the necessity to re-clone fusion constructs. In this study we designed four different anchors, yet hypothetically our system is compatible with any other desired subcellular targeting (Nelson et al., 2007). We have tested various FKBP-tagged bait POIs and successfully delocalized all of them to microtubules, to the plasma membrane, to the mitochondria and to the nucleus. We show that rapamycin-dependent FKBP-FRB

heterodimerization is robust and capable to trap POIs at an ectopic location. Also, re-routing is likely to occur faster than targeting to a specific location by conditionally expressing nanobodies (Früholz et al., 2018), as our approach does not rely on any translational step to achieve the delocalization. We observed rerouting of POIs in *N. benthamiana* within minutes, which is in agreement with very fast kinetics of FKBP-FRB binding upon rapamycin induction in *Arabidopsis* reported previously (Li et al., 2011).

KSP is a valuable tool to visualize PPI

We thoroughly investigated previously reported PPIs in KSP using mitochondrial and nuclear anchors. We prove that KPS is feasible for interactions holding diverse physiological roles in distinct biological processes. We successfully reproduced previously demonstrated interactions of the transcription factors SACL3 and LHW (Vera-Sirera et al., 2015),interplay of TPLATE and TML, subunits of endocytic TPLATE complex, (Gadeyne et al., 2014) and interaction between the brassinosteroid signaling proteins BIN2 and BES1 (Anwar et al., 2018; Planas-Riverola et al., 2019). Likewise, homodimerization of MAP65-1 (Tulin et al., 2012; Van Damme et al., 2004), could be identified using our system.

At the same time, in KSP PPIs visualize only upon drug exposure, which we consider one of the major advantages of our system, as this allows to omit performing additional control infiltrations. Rapamycin-induced visualization of interactions is at the same time rapid and long lasting. This allows POIs to be monitored throughout the entire experiment and visualization of PPI's can be drug-induced at any desired time point. The high affinity of the rapamycin dimerization (Banaszynski et al., 2005) however, makes it difficult to reverse. Ascomycin, a rapamycin competitor for HsFKBP (Paulmurugan et al., 2004) was shown to work also in plants (Li et al., 2011). Although we did not investigate the capacity of ascomycin to reverse the dimerization in this study, this could present a way if the delocalization would need to be reversed.

Another asset of KSP is its straightforward readout with reduced dependence on fluorophore choice, orientation and/or proximity. This is quite different from BiFC or FRET-FLIM assays where spatial tagging has a very prominent effect on the outcome of the interaction readout.

In addition, in contrast to BiFC, KSP is less prone to false positive results, which can be generated by, for example, unstable proteins.

Biological processes are regulated by many means, including higher-order cooperations between proteins. Evaluation of multimeric protein interplay remains a challenging task. Trifluorophore FRET-FLIM and trimolecular fluorescence complementation (Glöckner et al., 2019; Offenborn et al., 2015) have been shown to work in plants. The spatial tagging limitations required to have a positive readout using the above tools however are likely limiting to apply this for any random complex of choice. In contrast, our KSP system holds a great potential to visualize higher-order PPIs, which we were able to demonstrate for three members of the endocytic TPC. In theory, our system is compatible with even higher order interactions, and could contribute to insight into the TPC or other complexes structural properties.

Another great advantage of KSP lies in the quantification capabilities. We developed semi-automatic quantification scripts for mitochondrial (MitTally) and nuclear (NucTally) anchors. They produce straightforward results, expressed as an intensity ratio between particles (mitochondria or nuclei) and the cytoplasm. In addition, they provide both raw data results and results with outliers excluded via the interquartile range method. Both scripts require only moderate effort as pictures can be analyzed in batches, and results are easy to apply for statistical processing.

The limitation of the KSP system we encountered is that possibly, weak and transient interactions are not efficiently detected, as our POIs are not artificially coupled. The observed lack of interaction between CDKA;1 and KRP2 might be due to this pair's specific requirement of a nuclear environment or another interacting partner. Establishing spatial targeting inside the nucleus might help to solve this issue. Recently, TPX-Like proteins were shown to cause intranuclear MT polymerization i*n planta* (Boruc et al., 2019), therefore TPX-Likes could potentially be used in KSP as FRB* intranuclear anchor to visualize specific nuclear PPIs (Boruc et al., 2010b).

Future prospectives

We demonstrated that KSP can be used to visualize multiple proteins interactions. A logical next step would be to increase the number of interactors tested in a single assay. Especially, since the imaging of multiple fluorophores expressed together is becoming easier in the context of novel technical advances in confocal microscopy (Borlinghaus et al., 2006; Min et al., 2014). However, to infiltrate multiple constructs in *N. benthamiana* may lead to uneven expression patterns and ratios of these constructs. A solution would be combining expression of multiple proteins from a single vector to ensure the same expression levels of all of the co-expressed elements (Decaestecker et al., 2019; Engler et al., 2008; Sarrion-Perdigones et al., 2011).

KSP also has the potential to serve as an interactomics tool. Trapping FKBP-fused bait proteins and their interactors at the mitochondria could be combined with mitochondria isolation. Comparative mass spectrometry analysis of rapamycin-treated versus untreated samples will allow to analyze specific interacting partners. Recently, KS has been combined with the BioID into 2C-BioID in human fibroblast cells to conditionally target the biotin ligase to a specific subcellular location (Chojnowski et al., 2018). As the BioID has been recently adapted for plants (Arora et al., 2019) , 2C-BioID could be also introduced in planta, in order to improve the overall assay robustness.

KSP can also be further developed beyond a PPIs tool. Introducing KSP into other model systems like *Arabidopsis thaliana*, will create a possibility for conditional targeting of proteins and their interaction partners to a subcellular location. In animal cells, rapamycin-induced PM targeting of phosphatidylinositol phosphatases or AP-2 is used to acutely control endocytosis (Hammond et al., 2012; Heo et al., 2006; Wood et al., 2017). Possible applications in plants might therefore also include the acute and conditional targeting of proteases, kinases or phosphatases to a specific subcellular location.

Similar to KS in animals (Robinson et al., 2010), KSP might become a conditional *in planta* knockout tool, which could be used to study otherwise lethal mutants (Lloyd and Meinke, 2012; Lloyd et al., 2015). Even more, combining KSP with tissue-specific promoters (Siligato et al., 2016), would allow to live-image study the immediate effects of inducible protein knockouts in in particular plant cell types, tissues, and organs, while avoiding the pleiotropic effects of gene

loss by conventional approaches. This approach might overcome limitations in terms of capacity and/or timing observed by conditionally delocalizing functional proteins using nanobody expression (Winkler et al., 2020).

Taken together, our results show that KSP is robust and efficient tool for PPIs visualization in plants. As it holds specific advantages and can visualize higher order interactions, it will likely open a new route to investigate protein-protein interactions in plants complementary to the currently existing tools.

Materials and methods

Multisite Gateway cloning of entry clones

Gateway entry clones: pDONR221-TagBFP2, pDONR221-MITOTagBFP2, pDONR221MITO, pDONR221-MYRI, pDONR221-LHW, pDONR221-SACL3, pDONRP2RP3-FRB*, pDONRP2RP3-mCherry-FKBP and pENTR™ 5'-TOPO® entry clone: pUBQ10NLS were generated in this study according to the manufacturer's instructions (ThermoFisher Scientific BP clonase). pDONR221-TagBFP2 was amplified from pSN.5 mTagBFP2 (Pasin et al., 2014). pDONR221-MITOTagBFP2 was generated from pDONR221-TagBFP2 by including the import signal of the yeast mitochondrial outer membrane protein Tom70p as described before (Robinson et al., 2010). pDONR221-MITO was generated from pDONR221-MITOTagBFP2. pDONR221-MYRI, consisting of the N-terminal fragment (amino acids 1 to 76) of CPK34, which contains a myristylation/palmitoylation site (Kirik et al., 2012; Myers et al., 2009; Podell and Gribskov, 2004) was synthesized by Gen9 (now Ginkgo Bioworks, 27 Drydock Avenue, Boston, MA 02210). pDONR221-LHW and pDONR221-SACL3 (kindly provided by Prof. Bert De Rybel, PSB, Ghent, Belgium). pDONRP2RP3-mCherry-FKBP was generated by sewing PCR. First PCR was performed with mCherry-specific primers (Mylle et al., 2013). The forward primer contained the AttB2r site and the N-term mCherry sequence, the reverse primer contained the C-term mCherry sequence and the linker. The second PCR was made with the FKBP-specific domain (Robinson et al., 2010) primers. The forward primer contained the linker sequence and the N-term FKBP sequence and the reverse primer contained the C-term FKBP sequence flanked with AttB3. pDONRP2RP3-FRB* was amplified from MAPPER (Chang et al., 2013, 2017) with FRB* domain-

specific primers flanked with AttB2r and AttB3 sites. Star "*" stands for threonine 2098 to leucine mutation, which allows to replace rapamycin with its analogs – rapalogs (Bayle et al., 2006). pUBQ10NLS was generated using pUBQ forward and NLS reverse primers using the pBINU-NYA(K) (N799872) plasmid as template (Mehlmer et al., 2012). The overhangs were generated using Taq polymerase, and the purified amplicon was ligated into the pENTR 5'TOPO (ThermoFisher Scientific) according to manufacturer's instructions. The following entry clones were published before: pDONR207-EB1A, pDONR207-MAP65-1, pDONR207-T22.1/TPLATE (Van Damme et al., 2004), pDONR207-CLC1 At2g20760 (Van Damme et al., 2011), pDONR207-RCN1/PP2AA1 (Spinner et al., 2013), pDONR221-CDKA;1 (Boruc et al., 2010b), pDONR221-TASH3 (Gadeyne et al., 2014), pDONR221-BIN2, (Houbaert et al., 2018). All entry clones used in this study are listed in Supplemental Table 1: List of primers used.

All primers sequences are shown in Supplemental Table 1. Schematic representations of entry clones created *de novo* in this study are shown in Supplemental Figure 1.

LR binary vectors cloning

Gateway expression clones were obtained after LR recombination using LR clonase according to manufacturer's instructions (Thermo Fisher). CDKA;1-mCherry-FKBP, CLC2-mCherry-FKBP, EB1A-TagBFP-FRB, LHW-mCherry-FKBP, MAP-65-1-mCherry-FKBP, MITOTagBFP2-FRB, MYRI-TagBFP2FRB, pUBQ10NLS-TagBFP2-FRB, RCN1/PP2AA1-mCherry-FKBP, SACL3-GFP, TASH3-TagBFP2, TPLATE-mCherry-FKBP were cloned in pB7m34GW and under control of the p35S promoter, except MITOTagBFP2-FRB* and pUBQ10NLS-TagBFP2-FRB*. The two latter were cloned under control of pH3.3 (Ingouff et al., 2017) and pUBQ (Mehlmer et al., 2012) promoters respectively. The eGFP was cloned into the pK7WG2 (Karimi et al., 2002, 2005). The following expression clones were published before: pB7m34GW-pUBQ::GFP-AUXILIN-LIKE1 (Adamowski et al., 2018), pGWB6-GFP-FASS/TON2 (Spinner et al., 2013), pK7WG2-p35S::KRP2-GFP (Boruc et al., 2010b), pK7FWG2-35S::TML-GFP, pK7FWG2-p35S::LOLITA-GFP (Gadeyne et al., 2014), pK7FWG2-p35S::MAP65-1-GFP (Van Damme et al., 2004). 35S::BES1-GFP was a kind gift from Prof. Eugenia Russinova (PSB, Ghent, Belgium). All expression vectors and accession numbers are presented in Supplemental Table 2.

Plant growth and transient expression assay

Nicotiana benthamiana plants were grown in a greenhouse with long day conditions. Transient expression was performed by leaf infiltration (Sparkes et al., 2006) with modifications. *Agrobacterium* OD of MITOTagBFP2-FRB was adjusted to 0.1 prior mixing the cultures to assure sufficient protein expression while avoiding massive mitochondrial clustering. *N. benthamiana* leaves were imaged two days after infiltration. Imaging was performed on a PerkinElmer Ultraview spinning-disc system, attached to a Nikon Ti inverted microscope and operated using the Volocity software package. Images were acquired on an ImagEMccd camera (Hamamatsu C9100-13) using frame-sequential imaging with a 60x water immersion objective (NA = 1.20). Specific excitation and emission was performed using a 488nm laser combined with a single band pass filter (500-550nm) for GFP, 561nm laser excitation combined with a dual band pass filter (500-530nm and 570-625nm) for mCherry and 405nm laser excitation combined with a single band pass filter (454-496nm) for TagBFP2. Images shown are Z-stack projections, except the insets which represent enlarged, single slices (Figure 1A and B, Figure 2A, Figure 3B, Figure S3A). Z-stacks were acquired in sequential frame mode with a 1µm interval using the Ultraview (Piezo) focus drive module.

Drugs and mitochondrial marker treatment

48h after infiltration of *N. benthamiana* leaves, treatment with 1µM rapamycin (Sigma-Aldrich) and/or 50µM oryzalin (Sigma-Aldrich) or 250nM MitoTracker™ Red CMXRos (Thermo Fisher) was performed by infiltrating the chemicals. Stock solutions (1mM rapamycin, 20mM oryzalin and 1mM MitoTracker) were prepared by diluting corresponding amount in DMSO (dimethyl sulfoxide). Prior to the infiltration, final concentrations of the chemicals were diluted in MiliQ® water.

Delocalization ratio quantification and statistics

Raw pictures (16bit) in Figure 2, Figure 3, Figure 4, Supplemental Figure 2, Supplemental Figure 5, Supplemental Figure 3 and Supplemental Figure 4 were exported from Volocity (Perkin

Elmer) as single files with merged Z-planes and separate channels. Pictures were processed in Fiji (Schindelin et al., 2012) as described below (see Supplemental document 1). For the mitochondrial rerouting analysis, outliers were automatically removed by MitTally on the basis of particle median intensities in a single step interquartile computation. For the nuclear rerouting analysis, outliers were automatically removed by NucTally on the basis of average nucleus ROI intensity in a single step interquartile computation. Mitochondria or nuclear vs cytoplasm intensity ratios generated with MitTally or NucTally were analyzed in RStudio with R (RStudio, 2015) with ANOVA to account for heteroscedasticity. Post hoc pairwise comparison was performed with the package MULTCOMP utilizing the Tukey contrasts (Herberich et al., 2010).

Accession Numbers

The Arabidopsis Information Resource (TAIR) locus identifiers for the genes mentioned in this study are AUXILIN-LIKE1 (At4G12780), BES1 (At1G19350), BIN2 (At4G18710), CDKA;1 (At3G48750), CLC1 (At2G20760), EB1a (At3G47690), FASS/TON2 (At5G18580), KRP2 (At3G50630), LHW (At2G27230), LOLITA (At1G15370), MAP65-1 (At5G55230), MYRI/CPK34 (At5G19360), RCN1/PP2AA1 (At1G25490), SACL3 (At1G29950), T22.1/TPLATE (At3G01780), TASH3 (At2G07360), TML (At5G57460).

Supplemental Material

Supplemental Figure 1: Schematic representation of the available Multisite Gateway entry clones and expression constructs used in this study.

Supplemental Figure 2: MITO-TagBFP2-FRB* occasionally causes mitochondrial clustering without interfering with their capacity to recruit FKBP-fused proteins.

Supplemental Figure 3: Oryzalin does not relocalize MAP65-1 to the nuclei.

Supplemental Figure 4: Rapamycin treatment relocalizes interacting proteins rapidly and remains effective over long periods.

Supplemental Figure 5: KSP does not stabilize protein-protein interactions and visualizing interactions via delocalization therefore has limitations.

Supplemental Table 1: List of primers used.

Supplemental Table 2: List of constructs used.

Supplemental document 1: Manual of the quantification scripts.

Acknowledgements

The authors would like to thank Prof. Jiri Friml (IST, Klosterneuburg, Austria) and Dr. Sibu Simon (CEITEC, Brno, Czech Republic) for the help in initiating this project and many colleagues who have provided material for this work. pSN.5 mTagBFP2 was kindly provided by Dr. Fabio Pasin (Academia Sinica, Taipei, Taiwan). pDONR221-LHW and pDONR221-SACL3 were kindly provided by Prof. Bert De Rybel (PSB, Ghent, Belgium). The FKBP construct was kindly provided by Prof. Margaret Robinson (CIMR, Cambridge, UK). pB7m34GW-pUBQ::GFP-AUXILIN-LIKE1 was kindly provided by Dr. Maciek Adamowski (IST, Klosterneuburg, Austria). pGWB6-GFP-FASS/TON2 was kindly given by Dr. Martine Pastuglia (IJPPB Versailles, France). pDONR221-BIN2 and 35S::BES1-GFP were kindly provided by Prof. Jenny Russinova (PSB, Ghent, Belgium). Research in the Van Damme lab is supported by the European Research Council T-Rex project number 682436 and by the National Science Foundation Flanders (FWO; G009415N).

Declaration of Interests

The authors declare no competing interests.

References

Adamowski, M., Narasimhan, M., Kania, U., Glanc, M., De Jaeger, G., and Friml, J. (2018). A Functional Study of AUXILIN-LIKE1 and 2, Two Putative Clathrin Uncoating Factors in Arabidopsis. Plant Cell *30*, 700–716.

Alberti, S., Gitler, A.D., and Lindquist, S. (2007). A suite of Gateway® cloning vectors for high-throughput genetic analysis in Saccharomyces cerevisiae. Yeast Chichester Engl. *24*, 913–919.

Anwar, A., Liu, Y., Dong, R., Bai, L., Yu, X., and Li, Y. (2018). The physiological and molecular mechanism of brassinosteroid in response to stress: a review. Biol. Res. *51*.

Arabidopsis Interactome Mapping Consortium, A.I.M.C. (2011). Evidence for Network Evolution in an Arabidopsis Interactome Map. Science *333*, 601–607.

Arora, D., Abel, N.B., Liu, C., Damme, P.V., Vu, L.D., Tornkvist, A., Impens, F., Eeckhout, D., Goossens, A., Jaeger, G.D., et al. (2019). Establishment of Proximity-dependent Biotinylation Approaches in Different Plant Model Systems. BioRxiv 701425.

Banaszynski, L.A., Liu, C.W., and Wandless, T.J. (2005). Characterization of the FKBP·Rapamycin·FRB Ternary Complex. J. Am. Chem. Soc. *127*, 4715–4721.

Bayle, J.H., Grimley, J.S., Stankunas, K., Gestwicki, J.E., Wandless, T.J., and Crabtree, G.R. (2006). Rapamycin Analogs with Differential Binding Specificity Permit Orthogonal Control of Protein Activity. Chem. Biol. *13*, 99–107.

Bhat, R.A., Lahaye, T., and Panstruga, R. (2006). The visible touch: in planta visualization of protein-protein interactions by fluorophore-based methods. Plant Methods *2*, 12.

Borlinghaus, R., Gugel, H., Albertano, P., and Seyfried, V. (2006). Closing the spectral gap: The transition from fixed-parameter fluorescence to tunable devices in confocal microscopy. J.-A. Conchello, C.J. Cogswell, and T. Wilson, eds. (San Jose, CA), p. 60900T.

Boruc, J., Van den Daele, H., Hollunder, J., Rombauts, S., Mylle, E., Hilson, P., Inzé, D., De Veylder, L., and Russinova, E. (2010a). Functional Modules in the Arabidopsis Core Cell Cycle Binary Protein–Protein Interaction Network[W]. Plant Cell *22*, 1264–1280.

Boruc, J., Mylle, E., Duda, M., De Clercq, R., Rombauts, S., Geelen, D., Hilson, P., Inzé, D., Van Damme, D., and Russinova, E. (2010b). Systematic Localization of the Arabidopsis Core Cell Cycle Proteins Reveals Novel Cell Division Complexes. Plant Physiol. *152*, 553–565.

Boruc, J., Deng, X., Mylle, E., Besbrugge, N., Durme, M.V., Demidov, D., Tomaštíková, E.D., Tan, T.-R.C., Vandorpe, M., Eeckhout, D., et al. (2019). TPX2-LIKE PROTEIN3 Is the Primary Activator of α-Aurora Kinases and Is Essential for Embryogenesis. Plant Physiol. *180*, 1389–1405.

Bracha-Drori, K., Shichrur, K., Katz, A., Oliva, M., Angelovici, R., Yalovsky, S., and Ohad, N. (2004). Detection of protein–protein interactions in plants using bimolecular fluorescence complementation. Plant J. *40*, 419–427.

Branon, T.C., Bosch, J.A., Sanchez, A.D., Udeshi, N.D., Svinkina, T., Carr, S.A., Feldman, J.L., Perrimon, N., and Ting, A.Y. (2018). Efficient proximity labeling in living cells and organisms with TurboID. Nat. Biotechnol. *36*, 880–887.

Cabantous, S., Nguyen, H.B., Pedelacq, J.-D., Koraïchi, F., Chaudhary, A., Ganguly, K., Lockard, M.A., Favre, G., Terwilliger, T.C., and Waldo, G.S. (2013). A New Protein-Protein Interaction Sensor Based on Tripartite Split-GFP Association. Sci. Rep. *3*.

Chang, C.-L., Hsieh, T.-S., Yang, T.T., Rothberg, K.G., Azizoglu, D.B., Volk, E., Liao, J.-C., and Liou, J. (2013). Feedback Regulation of Receptor-Induced Ca2+ Signaling Mediated by E-Syt1 and Nir2 at Endoplasmic Reticulum-Plasma Membrane Junctions. Cell Rep. *5*, 813–825.

Chang, C.-L., Chen, Y.-J., and Liou, J. (2017). ER-Plasma Membrane Junctions: Why and How Do We Study Them? Biochim. Biophys. Acta *1864*, 1494–1506.

Chojnowski, A., Sobota, R.M., Ong, P.F., Xie, W., Wong, X., Dreesen, O., Burke, B., and Stewart, C.L. (2018). 2C-BioID: An Advanced Two Component BioID System for Precision Mapping of Protein Interactomes. IScience *10*, 40–52.

Conlan, B., Stoll, T., Gorman, J.J., Saur, I., and Rathjen, J.P. (2018). Development of a Rapid in planta BioID System as a Probe for Plasma Membrane-Associated Immunity Proteins. Front. Plant Sci. *9*, 1882.

Cottier, S., Mönig, T., Wang, Z., Svoboda, J., Boland, W., Kaiser, M., and Kombrink, E. (2011). The Yeast Three-Hybrid System as an Experimental Platform to Identify Proteins Interacting with Small Signaling Molecules in Plant Cells: Potential and Limitations. Front. Plant Sci. *2*.

Das, P.P., Macharia, M.W., Lin, Q., and Wong, S.-M. (2019). In planta proximity-dependent biotin identification (BioID) identifies a TMV replication co-chaperone NbSGT1 in the vicinity of 126 kDa replicase. J. Proteomics *204*, 103402.

Decaestecker, W., Buono, R.A., Pfeiffer, M.L., Vangheluwe, N., Jourquin, J., Karimi, M., Isterdael, G.V., Beeckman, T., Nowack, M.K., and Jacobs, T.B. (2019). CRISPR-TSKO: A Technique for Efficient Mutagenesis in Specific Cell Types, Tissues, or Organs in Arabidopsis. Plant Cell *31*, 2868–2887.

De Rybel, B., Möller, B., Yoshida, S., Grabowicz, I., Barbier de Reuille, P., Boeren, S., Smith, R.S., Borst, J.W., and Weijers, D. (2013). A bHLH Complex Controls Embryonic Vascular Tissue Establishment and Indeterminate Growth in Arabidopsis. Dev. Cell *24*, 426–437.

Dixon, A.S., and Lim, C.S. (2010). The nuclear translocation assay for intracellular protein-protein interactions and its application to the Bcr coiled-coil domain. BioTechniques *49*, 519–524.

Engler, C., Kandzia, R., and Marillonnet, S. (2008). A One Pot, One Step, Precision Cloning Method with High Throughput Capability. PLoS ONE *3*.

Erffelinck, M.-L., Ribeiro, B., Perassolo, M., Pauwels, L., Pollier, J., Storme, V., and Goossens, A. (2018). High-throughput yeast two-hybrid library screening using next generation sequencing. BioRxiv 368704.

Fields, S., and Song, O. (1989). A novel genetic system to detect protein–protein interactions. Nature *340*, 245–246.

Förster, T. (1948). Zwischenmolekulare Energiewanderung und Fluoreszenz. Ann. Phys. *437*, 55–75.

Früholz, S., Fäßler, F., Kolukisaoglu, Ü., and Pimpl, P. (2018). Nanobody-triggered lockdown of VSRs reveals ligand reloading in the Golgi. Nat. Commun. *9*.

Fukao, Y. (2012). Protein–Protein Interactions in Plants. Plant Cell Physiol. *53*, 617–625.

Gadella, T.W.J., Jovin, T.M., and Clegg, R.M. (1993). Fluorescence lifetime imaging microscopy (FLIM): Spatial resolution of microstructures on the nanosecond time scale. Biophys. Chem. *48*, 221–239.

Gadeyne, A., Sánchez-Rodríguez, C., Vanneste, S., Di Rubbo, S., Zauber, H., Vanneste, K., Van Leene, J., De Winne, N., Eeckhout, D., Persiau, G., et al. (2014). The TPLATE Adaptor Complex Drives Clathrin-Mediated Endocytosis in Plants. Cell *156*, 691–704.

Ghosh, I., Hamilton, A.D., and Regan, L. (2000). Antiparallel Leucine Zipper-Directed Protein Reassembly: Application to the Green Fluorescent Protein. J. Am. Chem. Soc. *122*, 5658–5659.

Glöckner, N., Oven-Krockhaus, S. zur, Wackenhut, F., Burmeister, M., Wanke, F., Holzwart, E., Meixner, A.J., Wolf, S., and Harter, K. (2019). Three-fluorophore FRET-FLIM enables the study of trimeric protein interactions and complex formation with nanoscale resolution in living plant cells. BioRxiv 722124.

Grefen, C., and Blatt, M.R. (2012). A 2in1 cloning system enables ratiometric bimolecular fluorescence complementation (rBiFC). BioTechniques *53*, 311–314.

Hammond, G.R.V., Fischer, M.J., Anderson, K.E., Holdich, J., Koteci, A., Balla, T., and Irvine, R.F. (2012). PI4P And PI(4,5)P2 Are Essential But Independent Lipid Determinants Of Membrane Identity. Science *337*, 727–730.

Haruki, H., Nishikawa, J., and Laemmli, U.K. (2008). The Anchor-Away Technique: Rapid, Conditional Establishment of Yeast Mutant Phenotypes. Mol. Cell *31*, 925–932.

Heo, W.D., Inoue, T., Park, W.S., Kim, M.L., Park, B.O., Wandless, T.J., and Meyer, T. (2006). PI(3,4,5)P3 and PI(4,5)P2 Lipids Target Proteins with Polybasic Clusters to the Plasma Membrane. Science *314*, 1458–1461.

Herberich, E., Sikorski, J., and Hothorn, T. (2010). A robust procedure for comparing multiple means under heteroscedasticity in unbalanced designs. PloS One *5*, e9788.

Hirst, J., Schlacht, A., Norcott, J.P., Traynor, D., Bloomfield, G., Antrobus, R., Kay, R.R., Dacks, J.B., and Robinson, M.S. (2014). Characterization of TSET, an ancient and widespread membrane trafficking complex. ELife *3*.

Houbaert, A., Zhang, C., Tiwari, M., Wang, K., de Marcos Serrano, A., Savatin, D.V., Urs, M.J., Zhiponova, M.K., Gudesblat, G.E., Vanhoutte, I., et al. (2018). POLAR-guided signalling complex assembly and localization drive asymmetric cell division. Nature *563*, 574–578.

Hu, C.-D., Chinenov, Y., and Kerppola, T.K. (2002). Visualization of Interactions among bZIP and Rel Family Proteins in Living Cells Using Bimolecular Fluorescence Complementation. Mol. Cell *9*, 789–798.

Hughes, K.R., and Waters, A.P. (2017). Rapid inducible protein displacement in Plasmodium in vivo and in vitro using knocksideways technology. Wellcome Open Res. *2*.

Ingouff, M., Selles, B., Michaud, C., Vu, T.M., Berger, F., Schorn, A.J., Autran, D., Van Durme, M., Nowack, M.K., Martienssen, R.A., et al. (2017). Live-cell analysis of DNA methylation during

sexual reproduction in Arabidopsis reveals context and sex-specific dynamics controlled by noncanonical RdDM. Genes Dev. *31*, 72–83.

Jones, A.M., Xuan, Y., Xu, M., Wang, R.-S., Ho, C.-H., Lalonde, S., You, C.H., Sardi, M.I., Parsa, S.A., Smith-Valle, E., et al. (2014). Border Control—A Membrane-Linked Interactome of Arabidopsis. Science *344*, 711–716.

Kaplan-Levy, R.N., Quon, T., O'Brien, M., Sappl, P.G., and Smyth, D.R. (2014). Functional domains of the PETAL LOSS protein, a trihelix transcription factor that represses regional growth in Arabidopsis thaliana. Plant J. *79*, 477–491.

Karimi, M., Inzé, D., and Depicker, A. (2002). GATEWAY^{TM} vectors for Agrobacterium-mediated plant transformation. Trends Plant Sci. *7*, 193–195.

Karimi, M., De Meyer, B., and Hilson, P. (2005). Modular cloning in plant cells. Trends Plant Sci. *10*, 103–105.

Kessels, M.M., and Qualmann, B. (2002). Syndapins integrate N-WASP in receptor-mediated endocytosis. EMBO J. *21*, 6083–6094.

Khan, M., Youn, J.-Y., Gingras, A.-C., Subramaniam, R., and Desveaux, D. (2018). In planta proximity dependent biotin identification (BioID). Sci. Rep. *8*, 1–8.

Kirik, A., Ehrhardt, D.W., and Kirik, V. (2012). TONNEAU2/FASS Regulates the Geometry of Microtubule Nucleation and Cortical Array Organization in Interphase Arabidopsis Cells[C][W]. Plant Cell *24*, 1158–1170.

Lampugnani, E.R., Wink, R.H., Persson, S., and Somssich, M. (2018). The Toolbox to Study Protein–Protein Interactions in Plants. Crit. Rev. Plant Sci. *37*, 308–334.

Li, J.-F., Bush, J., Xiong, Y., Li, L., and McCormack, M. (2011). Large-Scale Protein-Protein Interaction Analysis in Arabidopsis Mesophyll Protoplasts by Split Firefly Luciferase Complementation. PLoS ONE *6*.

Lin, Q., Zhou, Z., Luo, W., Fang, M., Li, M., and Li, H. (2017). Screening of Proximal and Interacting Proteins in Rice Protoplasts by Proximity-Dependent Biotinylation. Front. Plant Sci. *8*.

Lloyd, J., and Meinke, D. (2012). A Comprehensive Dataset of Genes with a Loss-of-Function Mutant Phenotype in Arabidopsis1[W][OA]. Plant Physiol. *158*, 1115–1129.

Lloyd, J.P., Seddon, A.E., Moghe, G.D., Simenc, M.C., and Shiu, S.-H. (2015). Characteristics of Plant Essential Genes Allow for within- and between-Species Prediction of Lethal Mutant Phenotypes[OPEN]. Plant Cell *27*, 2133–2147.

Lv, S., Miao, H., Luo, M., Li, Y., Wang, Q., Julie Lee, Y.-R., and Liu, B. (2017). CAPPI: A Cytoskeleton-Based Localization Assay Reports Protein-Protein Interaction in Living Cells by Fluorescence Microscopy. Mol. Plant *10*, 1473–1476.

Magliery, T.J., Wilson, C.G.M., Pan, W., Mishler, D., Ghosh, I., Hamilton, A.D., and Regan, L. (2005). Detecting Protein−Protein Interactions with a Green Fluorescent Protein Fragment Reassembly Trap: Scope and Mechanism. J. Am. Chem. Soc. *127*, 146–157.

Mair, A., Xu, S., Branon, T.C., Ting, A.Y., and Bergmann, D.C. (2019). Proximity labeling of protein complexes and cell type-specific organellar proteomes in Arabidopsis enabled by TurboID. BioRxiv 629675.

Maruta, N., Trusov, Y., and Botella, J.R. (2016). Yeast Three-Hybrid System for the Detection of Protein-Protein Interactions. In Plant Signal Transduction: Methods and Protocols, J.R. Botella, and M.A. Botella, eds. (New York, NY: Springer), pp. 145–154.

Masters, S.C. (2004). Co-Immunoprecipitation from Transfected Cells. In Protein-Protein Interactions: Methods and Applications, H. Fu, ed. (Totowa, NJ: Humana Press), pp. 337–348.

Mehlmer, N., Parvin, N., Hurst, C.H., Knight, M.R., Teige, M., and Vothknecht, U.C. (2012). A toolset of aequorin expression vectors for in planta studies of subcellular calcium concentrations in Arabidopsis thaliana. J. Exp. Bot. *63*, 1751–1761.

Min, J., Vonesch, C., Kirshner, H., Carlini, L., Olivier, N., Holden, S., Manley, S., Ye, J.C., and Unser, M. (2014). FALCON: fast and unbiased reconstruction of high-density super-resolution microscopy data. Sci. Rep. *4*, 1–9.

Miteva, Y.V., Budayeva, H.G., and Cristea, I.M. (2013). Proteomics-based methods for discovery, quantification, and validation of protein-protein interactions. Anal. Chem. *85*, 749–768.

Miura, K. (2018). An Overview of Current Methods to Confirm Protein-Protein Interactions. Protein Pept. Lett. *25*, 728–733.

Myers, C., Romanowsky, S.M., Barron, Y.D., Garg, S., Azuse, C.L., Curran, A., Davis, R.M., Hatton, J., Harmon, A.C., and Harper, J.F. (2009). Calcium-dependent protein kinases regulate polarized tip growth in pollen tubes. Plant J. *59*, 528–539.

Mylle, E., Codreanu, M.-C., Boruc, J., and Russinova, E. (2013). Emission spectra profiling of fluorescent proteins in living plant cells. 8.

Nelson, B.K., Cai, X., and Nebenführ, A. (2007). A multicolored set of in vivo organelle markers for co-localization studies in Arabidopsis and other plants. Plant J. *51*, 1126–1136.

Nomura, W., Matsumoto, D., Sugii, T., Kobayakawa, T., and Tamamura, H. (2018). Efficient and Orthogonal Transcription Regulation by Chemically Inducible Artificial Transcription Factors. Biochemistry *57*, 6452–6459.

Offenborn, J.N., Waadt, R., and Kudla, J. (2015). Visualization and translocation of ternary Calcineurin-A/Calcineurin-B/Calmodulin-2 protein complexes by dual-color trimolecular fluorescence complementation. New Phytol. *208*, 269–279.

Ohashi-Ito, K., and Bergmann, D.C. (2007). Regulation of the Arabidopsis root vascular initial population by LONESOME HIGHWAY. Development *134*, 2959–2968.

Pasin, F., Kulasekaran, S., Natale, P., Simón-Mateo, C., and García, J.A. (2014). Rapid fluorescent reporter quantification by leaf disc analysis and its application in plant-virus studies. Plant Methods *10*, 22.

Paulmurugan, R., Massoud, T.F., Huang, J., and Gambhir, S.S. (2004). Molecular imaging of drug-modulated protein-protein interactions in living subjects. Cancer Res. *64*, 2113–2119.

Piya, S., Shrestha, S.K., Binder, B., Stewart, C.N., and Hewezi, T. (2014). Protein-protein interaction and gene co-expression maps of ARFs and Aux/IAAs in Arabidopsis. Front. Plant Sci. *5*.

Planas-Riverola, A., Gupta, A., Betegón-Putze, I., Bosch, N., Ibañes, M., and Caño-Delgado, A.I. (2019). Brassinosteroid signaling in plant development and adaptation to stress. Development *146*.

Podell, S., and Gribskov, M. (2004). Predicting N-terminal myristoylation sites in plant proteins. BMC Genomics *5*, 37.

Putyrski, M., and Schultz, C. (2012). Protein translocation as a tool: The current rapamycin story. FEBS Lett. *586*, 2097–2105.

Ransone, L.J. (1995). Detection of protein-protein interactions by coimmunoprecipitation and dimerization. In Methods in Enzymology, (Academic Press), pp. 491–497.

Rigaut, G., Shevchenko, A., Rutz, B., Wilm, M., Mann, M., and Séraphin, B. (1999). A generic protein purification method for protein complex characterization and proteome exploration. Nat. Biotechnol. *17*, 1030–1032.

Robinson, M.S., Sahlender, D.A., and Foster, S.D. (2010). Rapid Inactivation of Proteins by Rapamycin-Induced Rerouting to Mitochondria. Dev. Cell *18*, 324–331.

Rosenfeldt, G., Viana, R.M., Mootz, H.D., von Arnim, A.G., and Batschauer, A. (2008). Chemically induced and light-independent cryptochrome photoreceptor activation. Mol. Plant *1*, 4–14.

Roux, K.J., Kim, D.I., Raida, M., and Burke, B. (2012). A promiscuous biotin ligase fusion protein identifies proximal and interacting proteins in mammalian cells. J. Cell Biol. *196*, 801–810.

RStudio (2015). RStudio: Integrated Development for R. RStudio, Inc., Boston, MA URL.

Rubio, V., Shen, Y., Saijo, Y., Liu, Y., Gusmaroli, G., Dinesh-Kumar, S.P., and Deng, X.W. (2005). An alternative tandem affinity purification strategy applied to Arabidopsis protein complex isolation. Plant J. *41*, 767–778.

Sarrion-Perdigones, A., Falconi, E.E., Zandalinas, S.I., Juárez, P., Fernández-del-Carmen, A., Granell, A., and Orzaez, D. (2011). GoldenBraid: An Iterative Cloning System for Standardized Assembly of Reusable Genetic Modules. PLOS ONE *6*, e21622.

Schindelin, J., Arganda-Carreras, I., Frise, E., Kaynig, V., Longair, M., Pietzsch, T., Preibisch, S., Rueden, C., Saalfeld, S., Schmid, B., et al. (2012). Fiji: an open-source platform for biological-image analysis. Nat. Methods *9*, 676–682.

Siligato, R., Wang, X., Yadav, S.R., Lehesranta, S., Ma, G., Ursache, R., Sevilem, I., Zhang, J., Gorte, M., Prasad, K., et al. (2016). MultiSite Gateway-Compatible Cell Type-Specific Gene-Inducible System for Plants1[OPEN]. Plant Physiol. *170*, 627–641.

Sparkes, I.A., Runions, J., Kearns, A., and Hawes, C. (2006). Rapid, transient expression of fluorescent fusion proteins in tobacco plants and generation of stably transformed plants. Nat. Protoc. *1*, 2019–2025.

Spinner, L., Gadeyne, A., Belcram, K., Goussot, M., Moison, M., Duroc, Y., Eeckhout, D., De Winne, N., Schaefer, E., Van De Slijke, E., et al. (2013). A protein phosphatase 2A complex spatially controls plant cell division. Nat. Commun. *4*, 1863.

Struk, S., Jacobs, A., Martín-Fontecha, E.S., Gevaert, K., Cubas, P., and Goormachtig, S. (2019). Exploring the protein–protein interaction landscape in plants. Plant Cell Environ. *42*, 387–409.

Sun, Y., Wallrabe, H., Seo, S.-A., and Periasamy, A. (2011). FRET microscopy in 2010: The legacy of Theodor Förster on the 100th anniversary of his birth. Chemphyschem Eur. J. Chem. Phys. Phys. Chem. *12*, 462–474.

Titeca, K., Lemmens, I., Tavernier, J., and Eyckerman, S. (2019). Discovering cellular protein-protein interactions: Technological strategies and opportunities. Mass Spectrom. Rev. *38*, 79–111.

Tulin, A., McClerklin, S., Huang, Y., and Dixit, R. (2012). Single-Molecule Analysis of the Microtubule Cross-Linking Protein MAP65-1 Reveals a Molecular Mechanism for Contact-Angle-Dependent Microtubule Bundling. Biophys. J. *102*, 802–809.

Van Damme, D., Bouget, F.-Y., Poucke, K.V., Inzé, D., and Geelen, D. (2004). Molecular dissection of plant cytokinesis and phragmoplast structure: a survey of GFP-tagged proteins. Plant J. *40*, 386–398.

Van Damme, D., Gadeyne, A., Vanstraelen, M., Inzé, D., Van Montagu, M.C.E., De Jaeger, G., Russinova, E., and Geelen, D. (2011). Adaptin-like protein TPLATE and clathrin recruitment during plant somatic cytokinesis occurs via two distinct pathways. Proc. Natl. Acad. Sci. U. S. A. *108*, 615–620.

Vera-Sirera, F., De Rybel, B., Úrbez, C., Kouklas, E., Pesquera, M., Álvarez-Mahecha, J.C., Minguet, E.G., Tuominen, H., Carbonell, J., Borst, J.W., et al. (2015). A bHLH-Based Feedback Loop Restricts Vascular Cell Proliferation in Plants. Dev. Cell *35*, 432–443.

Walter, M., Chaban, C., Schütze, K., Batistic, O., Weckermann, K., Näke, C., Blazevic, D., Grefen, C., Schumacher, K., Oecking, C., et al. (2004). Visualization of protein interactions in living plant cells using bimolecular fluorescence complementation. Plant J. *40*, 428–438.

Wen, C.-K. (2014). Ethylene in Plants (Springer).

Wiens, M.D., and Campbell, R.E. (2018). Surveying the landscape of optogenetic methods for detection of protein–protein interactions. Wiley Interdiscip. Rev. Syst. Biol. Med. *10*.

Winkler, J., Meyer, A.D., Mylle, E., Grones, P., and Damme, D.V. (2020). Nanobody-dependent delocalization of endocytic machinery in Arabidopsis root cells dampens their internalization capacity. BioRxiv 2020.02.27.968446.

Wood, L.A., Larocque, G., Clarke, N.I., Sarkar, S., and Royle, S.J. (2017). New tools for "hot-wiring" clathrin-mediated endocytosis with temporal and spatial precision. J. Cell Biol. *216*, 4351–4365.

Xing, S., Wallmeroth, N., Berendzen, K.W., and Grefen, C. (2016). Techniques for the Analysis of Protein-Protein Interactions in Vivo. Plant Physiol. *171*, 727–758.

Yang, F., Lei, Y., Zhou, M., Yao, Q., Han, Y., Wu, X., Zhong, W., Zhu, C., Xu, W., Tao, R., et al. (2018). Development and application of a recombination-based library versus library high-throughput yeast two-hybrid (RLL-Y2H) screening system. Nucleic Acids Res. *46*, e17.

Zhang, Y., Song, G., Lal, N.K., Nagalakshmi, U., Li, Y., Zheng, W., Huang, P.-J., Branon, T.C., Ting, A.Y., Walley, J.W., et al. (2019). TurboID-based proximity labeling reveals that UBR7 is a regulator of N NLR immune receptor-mediated immunity. Nat. Commun. *10*, 3252.

Figures

Figure 1

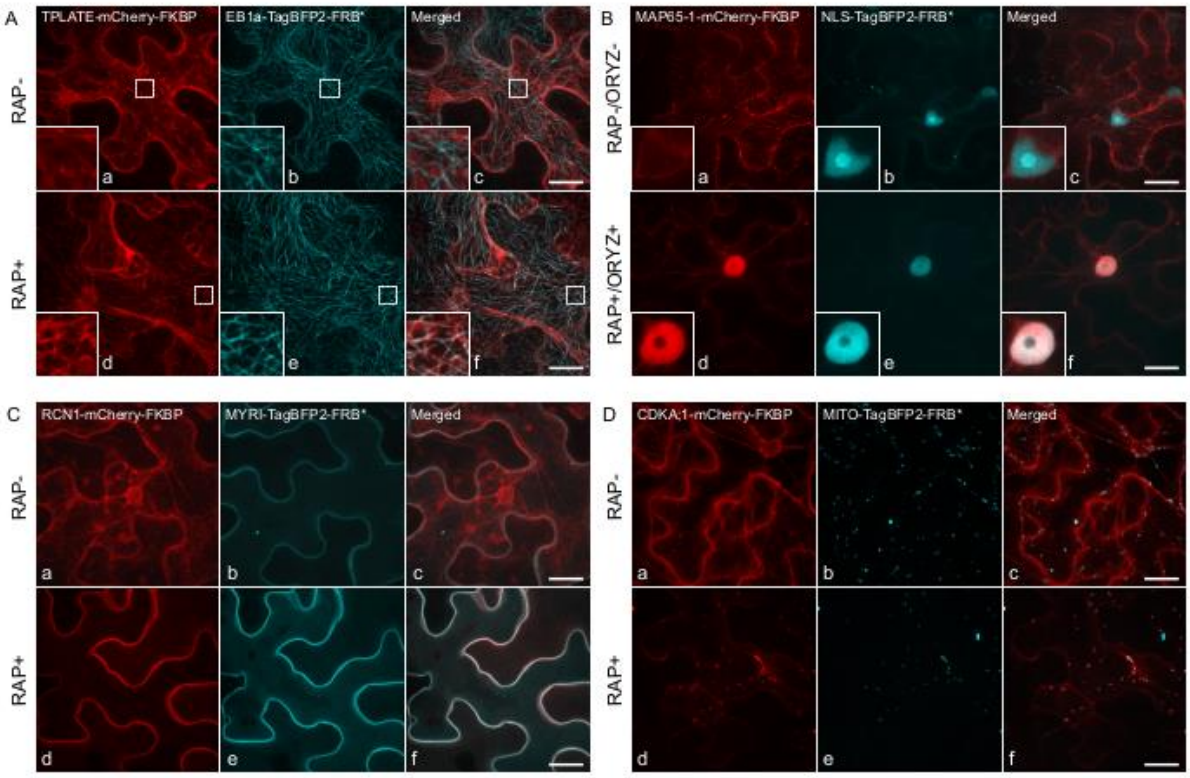

Figure 1: Rapamycin allows relocalization of FKBP protein fusions to different subcellular compartments in *Nicotiana benthamiana* epidermal leaf cells.

Representative Z-stack projections of epidermal *N. benthamiana* cells transiently expressing mCherry-FKBP and TagBFP2-FRB* fusion proteins in the absence (RAP-) or presence (RAP+) of rapamycin.

(A) Targeting to microtubules. Without rapamycin TPLATE-mCherry-FKBP localizes in the cytoplasm (a), while EB1a-TagBFP2-FRB* decorates microtubules (b). Rapamycin redirects TPLATE-mCherry-FKBP effectively to the microtubule cytoskeleton (d-f). The insets represent single-layer enlarged, contrast-enhanced microtubular areas.

(B) Targeting to the nucleus. Without rapamycin and oryzalin (ORYZ-), MAP65-1 labels the cortical microtubule cytoskeleton and is excluded from the nucleus (a). NLS-TagBFP2-FRB* strongly accumulates inside the nuclei (b). Oryzalin (ORYZ+) releases MAP65-1-mCherry-FKBP into the cytosol and rapamycin relocalizes it to the nuclei (d-f). The insets represent single-layer enlarged nuclear areas.

(C) Targeting to the plasma membrane. Without rapamycin, RCN1-mCherry-FKBP localizes in the cytoplasm and to the nuclei (a), while MYRI-TagBFP2-FRB* is exclusively at the plasma membrane (b). Rapamycin relocalizes RCN1-mCherry-FKBP effectively to the plasma membrane (d-f).

(D) Targeting to mitochondria. Without rapamycin, CDKA;1-mCherry-FKBP localizes predominantly in the cytoplasm (a) and does not co-localize with the mitochondrial targeted MITO-TagBFP2-FRB* (b). Following rapamycin treatment, CDKA;1-mCherry-FKBP is redirected to the mitochondria (d-f).

Images on the right contain the merged panels (c, f). Scale bars = 20µm.

Figure 2

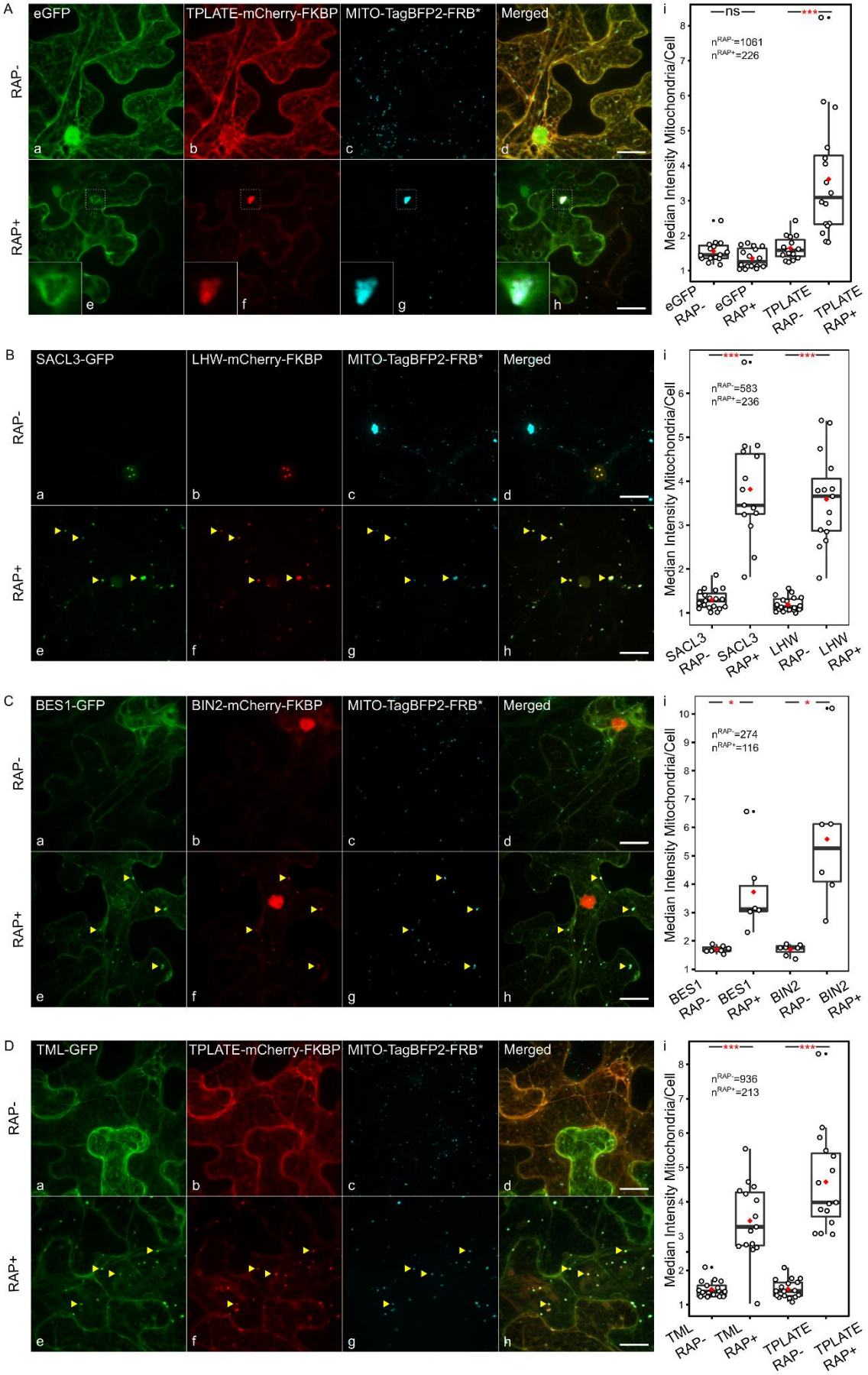
A
eGFP
TPLATE-mCherry-FKBP
MITO-TagBFP2-FRB*
Merged
RAP-
RAP+
a
b
c
d
e
f
g
h
i
ns
***
n^RAP-=1061
n^RAP+=226
Median Intensity Mitochondria/Cell
eGFP RAP-
eGFP RAP+
TPLATE RAP-
TPLATE RAP+
B
SACL3-GFP
LHW-mCherry-FKBP
MITO-TagBFP2-FRB*
Merged
n^RAP-=583
n^RAP+=236
SACL3 RAP-
SACL3 RAP+
LHW RAP-
LHW RAP+
C
BES1-GFP
BIN2-mCherry-FKBP
MITO-TagBFP2-FRB*
Merged
n^RAP-=274
n^RAP+=116
BES1 RAP-
BES1 RAP+
BIN2 RAP-
BIN2 RAP+
D
TML-GFP
TPLATE-mCherry-FKBP
MITO-TagBFP2-FRB*
Merged
n^RAP-=936
n^RAP+=213
TML RAP-
TML RAP+
TPLATE RAP-
TPLATE RAP+

Figure 2: KSP allows quantitative visualization of protein-protein interactions in plants via delocalization to mitochondria.

(A-D) Representative Z-stack projected images of epidermal *N. benthamiana* cells transiently expressing various GFP-fused proteins (a, e), mCherry-FKBP-fused proteins (b, f) and TagBFP2-FRB* construct targeted to the mitochondria (c, g). Panels on the right represent merged images (d, h). The free-GFP does not co-localize with the mCherry- and TagBFP2-positive mitochondria of which some are clustered both in the absence (RAP-) and presence (RAP+) of rapamycin (A). In the absence of rapamycin (RAP-), none of the GFP or mCherry fused proteins co-localize with the TagBFP2-FRB* constructs. After rapamycin treatment, FKBP protein fusions are effectively relocalized to the mitochondria (B-C, yellow arrowheads), confirming their interaction with the FKBP-fused bait protein. The insets represent an enlarged, single-layer cytosolic area surrounding a mitochondrial cluster (A). Scale bars = 20µm. $n^{RAP-/RAP+}$ refers to the total number of analyzed mitochondria in untreated (RAP-) or rapamycin-exposure (RAP+) conditions. Statistical analysis (panels i) is shown as box plot and jitter box, where the black line represents the median and red diamond represents the mean of the analyzed values. Each dot represents an individual picture. P-values <0.001 are represented as ***, <0.01 as ** and <0.05 as *. Not statistically significant results are notes as 'ns'. Statistical test was performed with ANOVA to account for heteroscedasticity. Post hoc pairwise comparison was performed with the package MULTCOMP utilizing the Tukey contrasts.

Figure 3

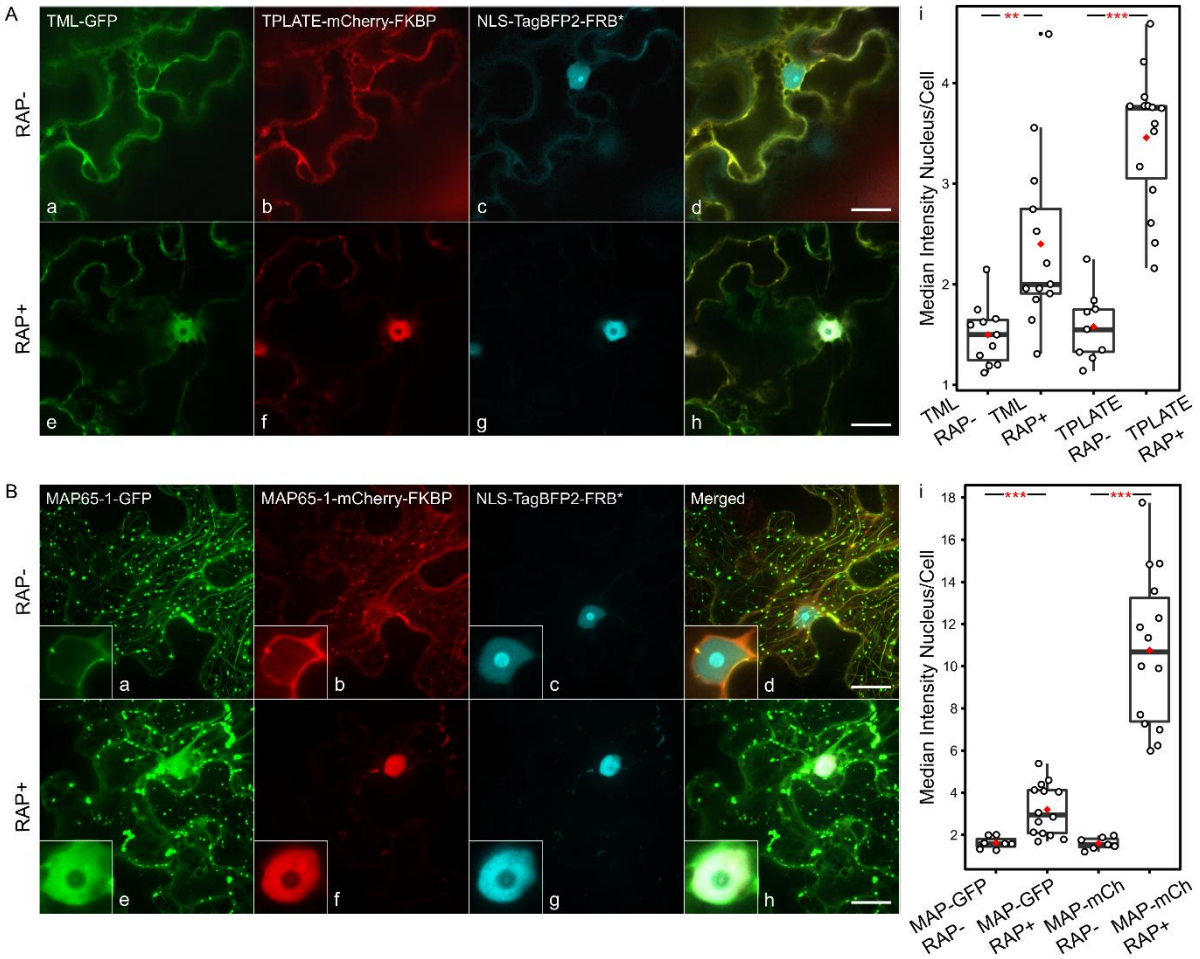

Figure 3: KSP allows quantitative visualization of protein-protein interactions in plants via delocalization to the nucleus.

(A-B) Representative Z-stack projected images of epidermal *N. benthamiana* cells transiently expressing various GFP-fused proteins (a, e), mCherry-FKBP-fused proteins (b, f) and NLS-TagBFP2-FRB* targeted to the nuclei (c, g). Panels on the right represent merged images (d, h). In the absence of rapamycin (RAP-), localization of the GFP or mCherry fused proteins remains unchanged and irrespective of the nuclear-localized TagBFP2-FRB* construct. Rapamycin effectively relocalizes FKBP fusions to the nuclei and consequently also the interacting -GFP fused proteins. The insets represent an enlarged, nuclear area (B). Scale bars = 20µm. Statistical analysis (panels i) is shown as box plot and jitter box, where the black line represents the median and red diamond represents the mean of the analyzed values. Each dot represents an individual picture. P-values <0.001 are represented as ***, <0.01 as ** and <0.05 as *. Statistical test was performed with ANOVA to account for heteroscedasticity. Post hoc pairwise comparison was performed with the package MULTCOMP utilizing the Tukey contrasts.

Figure 4

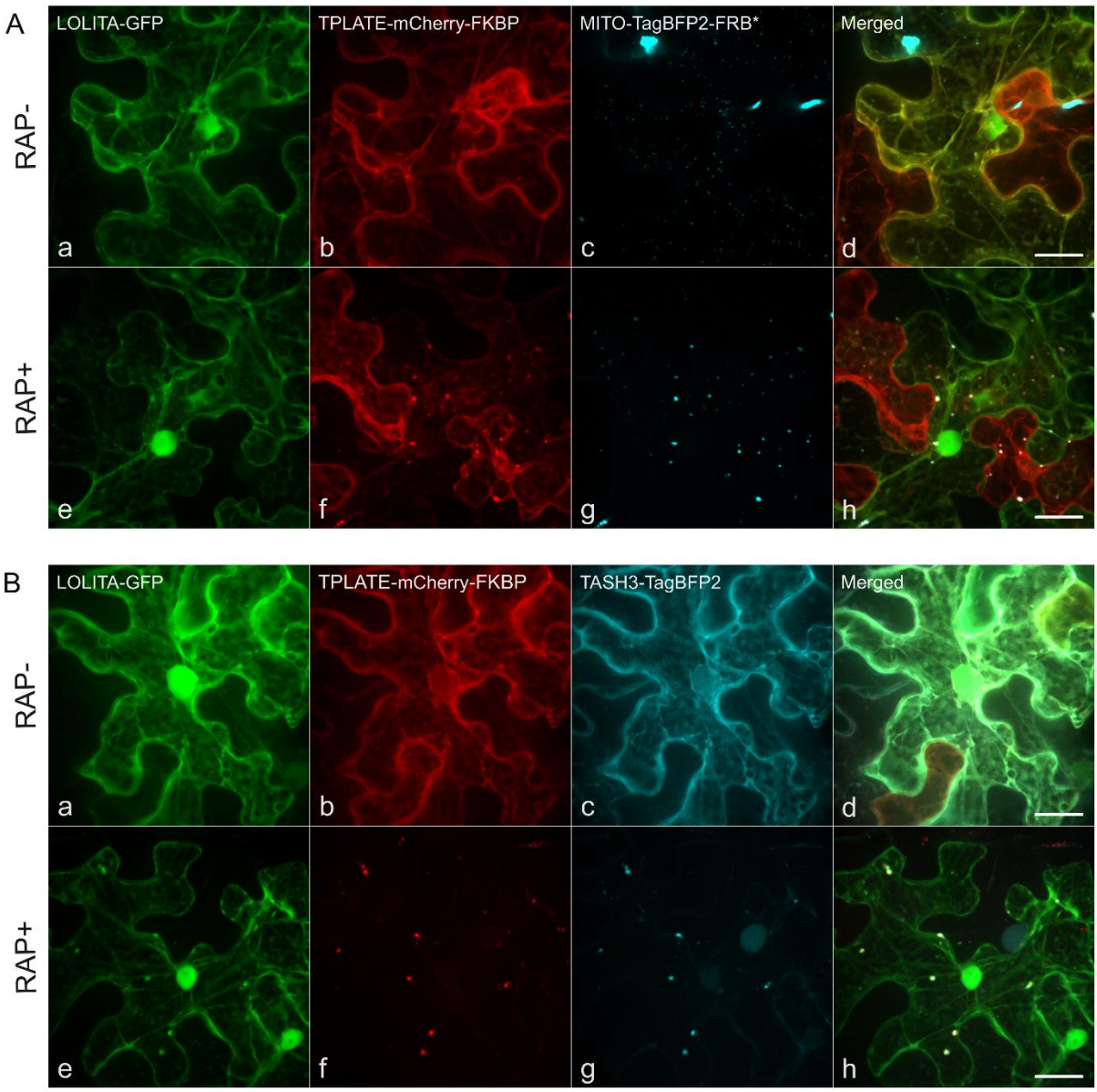

Figure 4: KSP allows visualizing higher order protein-protein interactions *in planta*.

(A) Representative Z-stack projections of *N. benthamiana* cells transiently expressing LOLITA-GFP (a, e), TPLATE-mCherry-FKBP (b, f), MITO-TagBFP2-FRB* (c, g) and the merged images (d, h), in the absence (RAP-) or presence (RAP+) of rapamycin. Following rapamycin treatment, TPLATE-mCherry-FKBP (f) relocalizes from the cytoplasm to the mitochondria (g), while the nuclear and cytoplasmic localization of LOLITA-GFP remains unchanged (e).

(B) Representative Z-stack projections of cells transiently expressing LOLITA-GFP (a, e) TPLATE-mCherry-FKBP (b, f) TASH3-TagBFP2 (c, g) as well as MITO-FRB* without fluorescent label, in the absence (RAP-) and presence (RAP+) of rapamycin. Introduction of TASH3-TagBFP2 as third partner stabilizes the interaction between LOLITA-GFP and TPLATE-mCherry-FKBP and allows all three proteins to relocalize to the mitochondria after rapamycin treatment (RAP+) (d, h). Scale bars = 20µm.